Molecular Therapy
Methods & Clinical Development
Original Article

Comparative assessment of the transduction efficiency and safety associated with the delivery of AAV9-GFP vector via lumbar puncture to cynomolgus macaques with and without anti-AAV9 pre-existing antibodies

Ghiabe H. Guibinga,[1,2] Janet Do,[1] Binh Chu,[1] Yin Gu,[1,2] Rie Kikkawa,[3] Xiaoguang Li,[2] Fatih Ozsolak,[1,2] and Timothy MacLachlan[4]

[1]Novartis Gene Therapies, San Diego, CA, USA; [2]Biologics Research Center (BRC), Novartis Biomedical Research, San Diego, CA, USA; [3]Preclinical Safety (PCS), Novartis Biomedical Research, East Hanover, NJ, USA; [4]Preclinical Safety (PCS), Novartis Biomedical Research, Cambridge, MA, USA

Administration of AAV-based gene therapies into the intra-cerebrospinal fluid (CSF) compartments via routes such as lumbar puncture (LP) has been implemented as an alternative to intravenous dosing to target the CNS regions. This route enables lower doses, decreases systemic toxicity, and circumvents intravascular pre-existing anti-AAV antibodies. In this study, AAV9-GFP vectors were administered via LP to juvenile cynomolgus macaques with and without pre-existing serum anti-AAV9 antibodies at a 5.0 × 10^{13} vector genomes per mL (vg/mL) dose and examined for 28 days. CNS and peripheral tissues were surveyed for vector genome, mRNA, and protein expression. Histopathology, clinical pathology, and humoral immune response to the viral capsid and transgene were also assessed. In addition, serum and CSF samples were analyzed to examine 276 proteomic markers curated to evaluate neural injury, organ damage, and inflammatory response. This study reveals no noticeable difference in AAV9-mediated gene transfer in the CNS tissues in the two groups; however, differences were observed for endpoints such as liver enzyme activities, histopathology, and levels of protein markers in the serum and CSF. These findings provide a view into vector transduction efficiency and safety following LP-delivered AAV9 to juvenile cynomolgus macaques with and without pre-existing anti-AAV9 antibodies.

INTRODUCTION

Pre-existing immunity to AAVs is thought to emerge in animals and humans from natural exposure to wild-type AAV serotypes. Anti-AAV antibodies resulting from this exposure can effectively hinder successful AAV-based gene therapy by interfering with gene transfer, especially when delivered intravenously (i.v.).[1,2] The intra-cerebrospinal fluid (CSF) delivery of AAV therapeutics through either lumbar puncture (LP), intra-cisterna magna, or intracerebroventricular routes have been explored as alternative options to i.v. dosing for administering vectors intended for CNS transduction.[3–5] These routes of AAV administration have been used in numerous nonclinical and clinical studies.[3,6–9] The few potential advantages of using an intra-CSF route for AAV vector administration include circumventing the need for large doses and potentially gaining more direct access to the CNS regions. In addition, evasion of pre-existing anti-AAV antibodies in blood and other compartments is also a potential benefit.[4] While pre-screening for anti-AAV9 antibodies is readily performed before intra-CSF dosing in several nonclinical large animal studies,[10–12] it is not considered as critical as for intravenous dosing, where there is more documented evidence that pre-existing antibodies hinder the efficacy of AAV-based therapeutics.[13,14]

For nonclinical studies in large animal models using intra-CSF AAV vector administration, it is believed that anti-AAV pre-existing antibodies do not to interfere or have a limited impact on CNS transduction.[4,6,7] Furthermore, several AAV gene therapy clinical trials using intra-CSF administration do not include anti-AAV titers as part of enrollment criteria (i.e., NCT04737460, CLN7 Disease; NCT05518188, Spastic Paraplegia type 50 [SPG50]; NTC02362438, Giant Axonal Neuropathy [GAN]). While it has been considered that AAV vectors delivered via the intrathecal route are shielded partly from anti-AAV antibodies present in the systemic circulation,[4] there is now an emerging consensus that vector delivered via the

Received 29 February 2024; accepted 4 November 2024;
https://doi.org/10.1016/j.omtm.2024.101371.

Correspondence: Ghiabe H. Guibinga, Biologics Research Center (BRC), Novartis Biomedical Research, 10210 Campus Point Dr Suite 350, San Diego, CA 92121, USA. E-mail:
E-mail: ghiabe.guibinga@novartis.com
Correspondence: Fatih Ozsolak, Biologics Research Center (BRC), Novartis Biomedical Research, 10210 Campus Point Dr Suite 350, San Diego, CA 92121, USA. E-mail:
E-mail: fatih.ozsolak@novartis.com

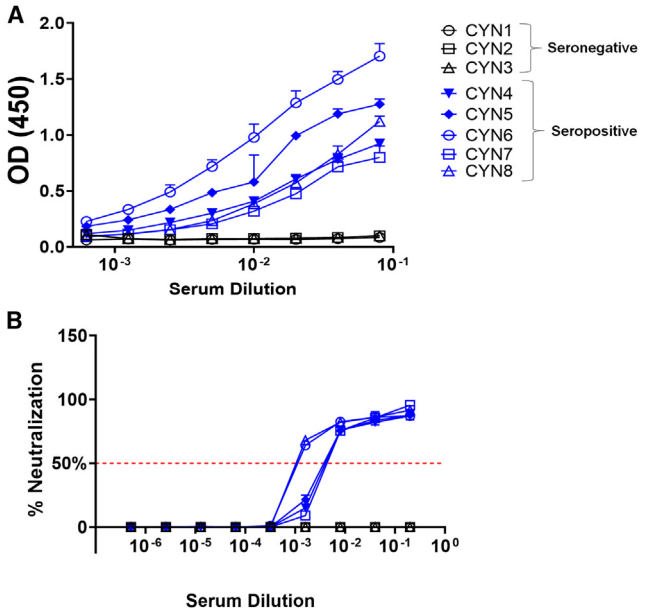

Figure 1. Selection and classification of NHP based on screening for pre-existing anti-AAV9 IgG binding antibodies and neutralizing antibodies

NHP serum samples were screened by ELISA and neutralization *in vitro* reporter assay.

(A) ELISA for anti-AAV9 IgG antibodies in the serum samples of non-human primates prior to dosing (pre-screening). Binding curves indicate the absence of binding antibodies in three animals (CYN1, CYN2, and CYN3), classified henceforth as seronegative. The presence of binding antibodies is observed in five animals (CYN4, CYN5, CYN6, CYN7, and CYN8), classified henceforth as seropositive. (B) The same serum samples were subsequently screened for anti-AAV9-neutralizing antibodies using an *in vitro* luciferase reporter system. Neutralizing curves indicate that sera from seronegative animals do not display neutralization activity, while sera from seropositive animals show the presence the presence of neutralizing antibodies. All data are presented as mean ± standard deviation (SD) (three technical triplicates).

intra-CSF route can leak into peripheral organs.[15,16] In this regard, it may be essential to re-evaluate how vector transduction efficiency and safety following intra-CSF delivery of AAVs varies in subjects based on the presence of anti-AAV9 serum antibodies at the time of dosing.

In this study, we hypothesize that presence or absence of anti-AAV9 neutralizing antibodies before intrathecal AAV9 dosing in NHP may impart difference in study metrics that inform efficacy and toxicity. Therefore, we have assessed a series of endpoints that inform transduction efficiency *in vivo* and safety of AAV9-based gene therapies. We identified noticeable differences between animals with and without anti-AAV9 serum neutralizing antibodies prior to AAV9 dosing, especially as it pertains to liver enzymes, histopathology findings, and AAV9-mediated gene transfer in peripheral organs. Also, using the Olink proteomics platform, we examined the serum and CSF samples of these animals for 276 protein markers curated to inform neural injury, organ damage, and inflammatory events. The analysis shows potential differences in levels of several markers between these two groups. The data provide novel insights into vector transduction efficiency and toxicity endpoints assessment in nonclinical animal study models based on their anti-AAV9 serology status at the time of intra-CSF dosing of AAV9 vectors.

RESULTS

Animal selection and AAV9 pre-existing antibody status

Serum samples from juvenile male cynomolgus macaques, all less than 3 years, were pre-screened for the presence of pre-existing anti-AAV9 antibodies using two distinct assays: a binding IgG antibody ELISA assay, which assessed the level of binding antibodies (BAbs), and an *in vitro* reporter assay to evaluate the level of neutralization antibodies (NAbs). Both assays were run based on concepts and methods described previously.[17–20] Figures 1A and 1B show the total IgG antibody binding curves and the NAb curves, respectively, of the eight NHPs prior to AAV9 dosing. The serum of three out of eight of these animals (CYN1, CYN2, and CYN3) displayed almost no level of AAV9 antigen binding; the sera of the same animals also indicate absence of neutralizing activities—these animals were classified and referred to henceforth as seronegative. Five of the remaining animals (CYN4, CYN5, CYN6, CYN7, and CYN8) showed evidence of pre-existing anti-AAV9 antibodies, as indicated by the antigen binding and neutralization curves—these animals were classified and referred henceforth as seropositive (see Figures 1A and 1B). BAb titers indicated in Table 1 were estimated as the last dilution with optical density (OD) reading 7- to 8-fold over the background. Meanwhile NAb titers were estimated as the last dilution with at least 50% reduction of luciferase expression (i.e., neutralizing activity). Total serum anti-AAV9 IgM antibodies were also assessed in NHPs before dosing. Data indicate the presence of IgM antibodies in the sera of seropositive animals and lack thereof in their seronegative counterparts (Figure S1). Overall, the BAb and NAb assay data outlined in this section clearly delineate the two groups of NHP based on the absence and the presence of pre-existing anti-AAV9 antibodies.

Safety and clinical pathology

LP administration of AAV9-GFP at 5.0×10^{13} vector genomes (vg) per NHP was well tolerated, with no evidence of acute clinical toxicity for both groups following dosing. All eight animals survived until their terminal necropsy 28 days post-injection, with no test article-related clinical observations or effects on food consumption as assessed qualitatively. All animals display no weight loss with no significant changes in body weight during the study. Clinical pathology assessments, including hematology, coagulation, and clinical chemistry, were carried out prior to dosing (day 0) and weekly on days 7, 14, 21, and 28, the day of scheduled euthanasia. Forty-two clinical pathology parameters were evaluated during the study (Table S1). Most of these markers fell within normal limits except for the liver transaminase activities of alanine transferase (ALT) and aspartate transferase (AST) of the seronegative animals in comparison with their seropositive counterparts (Figures 2A and 2B). Based on these differences in acute elevation of ALT and AST enzyme activities between the seropositive and seronegative group, these data argue that the presence of pre-existing anti-AAV9 NAb is protective of acute liver toxicity.

Table 1. NHPs used in this study

	Experiment ID	CYN ID	Gender	Age (years)	Total BAb titer	NAb titer
Seronegative	L21[a]	CYN1	M	2.6	<1:12.5	<1:5
	L22[a]	CYN2	M	2.5	<1:12.5	<1:5
	L23[a]	CYN3	M	2.8	<1:12.5	<1:5
Seropositive	L24[a]	CYN4	M	2.7	1:100	1:625
	L31	CYN5	M	24	1:200	1:625
	L32	CYN6	M	2.9	1:400	1:3125
	L33	CYN7	M	2.6	1:50	1:625
	L34	CYN8	M	2.9	1:100	1:3125

NHP groups, with animal identifier, age, and total binding anti-AAV9 IgG antibody (BAb) titers and anti-AAV9 neutralizing antibody (NAb) titers in the serum at the time of dosing.
[a]Animals were dosed 4 weeks apart from the others.

Evaluation of vector genome biodistribution and mRNA/protein expression

CNS tissues that include several areas of the brain and spinal cord and other peripheral tissues were collected and analyzed for vector genome, mRNA, and GFP transgene protein level. Vector genome was detected in the brain and spinal cord at various levels for both seronegative and seropositive animals with no apparent difference between the groups (Figure 3A). In peripheral tissues, however, a lower level of vector genome biodistribution in seropositive animals compared with their seronegative counterparts was observed (Figure 3B), with higher levels of vector DNA and transgene mRNA/protein in seronegative animals (Figures 3C–3E). These data confirm the restricting impact that the presence of anti-AAV9 neutralizing antibodies prior to IT/LP AAV9 dosage have in reducing AAV peripheral organ transduction, while minimally affecting the CNS compartment.

Anti-AAV9 capsid and anti-GFP IgG immune response

NHP serum samples were collected at days 0 (predose), 7, 14, 21, and 28, while CSF samples were collected at days 0, 7, and 28. Figure 4 summarizes the time course of endpoint titers, with fold dilution change differences between seronegative and seropositive animals. Higher anti-AAV9 antibody titers were observed in seropositive animals in serum and CSF compared with seronegative animals (Figures 4A and 4B), this is indicative of memory/recall immune response in seropositive animals. Meanwhile, anti-GFP antibody responses in seronegative animals trended higher (Figures 4C and 4D), this reflects higher GFP expression in this group observed in Figure 3. The antibody responses in the CSF for both GFP and AAV9 as assessed by endpoint titers is less accentuated in comparison with the one in the serum (Figures 4A–4D). This may reflect the difference in volume and fluid turnover rate of these two matrices/compartments. Overall, the robust anti-IgG antibody immune response mounted by the seropositive and seronegative NHP directed to the AAV9 capsid and the transgene reflects pre-exposure to AAV9 and GFP biodistribution in the respective group.

Microscopic observations

Tissues from all eight cynomolgus macaques collected in 10% neutral buffered formalin were evaluated to compare microscopic morphological features between seronegative and seropositive animals. Microscopic findings were observed in four categories (1) vector dosing-related changes observed with higher incidence/severity in seronegative animals, (2) vector-related changes observed with higher incidence/severity in seropositive animals, (3) vector-related changes comparably observed in both groups of animals, and (4) tissues with no vector-related change in either group based on historical analysis of animals dosed with vehicle only control.

Microscopic findings in this study observed upon dosing of AAV9 in NHPs included the CNS, dorsal root ganglion (DRG), and pancreas. Some findings, especially for the ones in peripheral tissues, were only observed in seronegative NHPs. This might possibly be due to higher biodistribution of AAV9 vectors as well as GFP transgene expression in seronegative animals. Seronegative animals had also an overall increased incidence and severity of mononuclear cell infiltration in choroid plexus, vascular/perivascular, meninges, and/or epineurium tissues. We observed, in the brain, neural degeneration and mononuclear cell infiltration in the lumbar and sacral DRG. Gliosis was also noted in the midbrain and brainstem (for summary, see Table S2; Figures 5A and 5B). In seropositive animals, the most characteristic changes observed were minimal to mild mononuclear cell infiltration in the vascular/perivascular region in the brain. Also noted was an increased occurrence of minimal axonal degeneration in the white matter (dorsal or lateral funiculi) in the thoracic and lumbar spinal cord, nerve root of the lumbar and sacral spinal cord, and thoracic DRG. Overall, many of these changes were of minimal severity and could be observed as background or incidental in cynomolgus monkeys (Table S3; Figures 5C and 5D). Vector-related changes that were observed comparably in both groups included gliosis in the cerebral cortex, spinal cord and/or DRGs, and mononuclear cell infiltration around the neuron of the cervical and thoracic DRGs, as well as in the pancreas, as indicated in Table S4 and Figure 5E. There were no AAV9-GFP-related microscopic findings in the liver, lung, quadriceps, femoris muscle, diaphragm, gastrointestinal tract (stomach, jejunum, and colon), and testis in either group of animals (Table S5). Overall, the histopathological data point to similitude and difference for the respective groups of treated NHPs in relation to the presence or absence of anti-AAV9 serum neutralizing antibodies prior to AAV9 dosing.

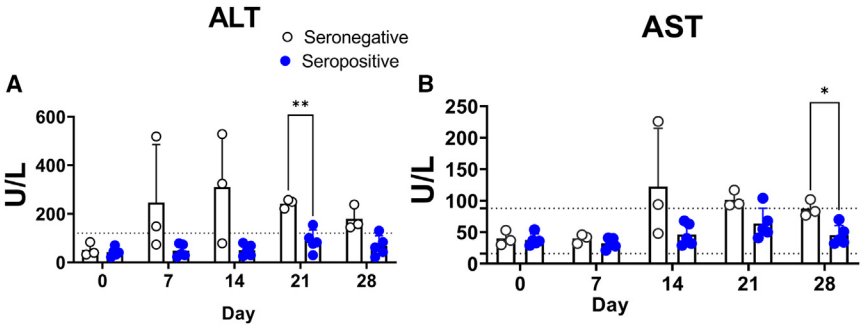

Figure 2. Liver enzyme activities (U/L) in seropositive and seronegative NHPs dosed via lumbar puncture at 5 × 10^{13} vg of AAV9-GFP vectors and examined for 28 days

Time course of (A) alanine aminotransferase (ALT) and (B) aspartate aminotransferase (AST) activities in seronegative (n = 3) and seropositive (n = 5) NHP serum samples following intra-CSF (lumbar puncture) delivery of 5 × 10^{13} vg of AAV9-GFP vectors. Data are presented as mean enzyme activity ± standard deviation (SD). The punctate line denotes the normal range. Where indicated, *p < 0.05 (two-way ANOVA Sidak's multiple comparison test).

Cytokines and other protein marker analyses

We examined the level of cytokines and other markers in the serum and CSF of dosed animals. We inferred that divergent protein expression, especially in peripheral tissues, and the differing immune response to AAV9 and GFP between seronegative and seropositive animals, may also lead to a different pattern of circulating protein levels. First, we used electrochemiluminescence (ECL)/meso-scale discovery (MSD) and ELISA bioassays to measure levels of cytokines (i.e., INF-γ, IL-1β, IL-2, IL-6, IL-8, and IL-10), neurofilament light (NfL), and neopterin in the serum and CSF of dosed animals on days 0, 7, and 28. While 7 days post-dose may not capture acute increases in cytokines, these time points may reflect residual inflammation. The levels of many of these markers were below the level of detection in the serum or the CSF at the indicated time points, except for IL-6, IL-8, and NfL, neopterin. In a subset of animals, there appears to be transient elevation of IL-6 in the CSF at day 7 for seropositive animals relative to their seronegative counterparts (Figure S2). Observable changes in NfL levels are also seen in the CSF of seropositive animals compared with the seronegative ones (Figure S3).

We expanded the breadth of this analysis by examining protein markers associated with inflammation and organ damage in the serum that may inform toxicity differences among seronegative and seropositive animals more accurately. Panels related to inflammation and organ damage containing 184 protein markers (see www.olink.com) were tested in the NHP serum samples collected at days 0, 7, and 28.

The analysis consisted of examining the difference in protein content within a given matrix (serum or CSF) between time points predose (day 0) and days 7 or 28. For the time point between days 0 and 7, four protein markers changed in the serum above the 2-fold cutoff for the combined seronegative and seropositive animals. Among the most noticeable change was the 2.78-fold drop in fibroblast growth factor 21 (FGF21) in seropositive animals (Table S6). Meanwhile, between days 0 and 28, 36 markers in the serum changed by at least 2-fold for both groups.

We further classified the protein changes in the serum into three categories (Figure 6A). The first category includes markers that change by at least 2-fold in the seronegative group only, among them there were 19 serum markers with content level above this 2-fold cutoff. Among the top dysregulated markers with statistically significant increase in level content were cardiac troponin (*TNNI3*), pleiotrophin (*PTN*), and the chemokines CXCL10 and CCL20, as well as pro-inflammatory cytokines such as TNF-α and IL-18 (Figure 6B). All the dysregulated proteins for this first category are summarized in Table S7. The second category were proteins that change by at least a median 2-fold only in the seropositive group. One of the protein markers with the most disrupted content in the serum was FK506 binding protein 1B (*FKBP1B*), with a content level that increases by 7.6-fold in seropositive monkeys versus 1.46 in their seronegative counterparts, a trend that did not reach statistical significance (p = 0.143) (Figure 6C). All the dysregulated proteins for this second category are summarized in Table S8. The third category includes markers that change in both seronegative and seropositive groups. The most noticeable changes in this group were seen for the chemokine CXCL9, which increases more significantly between days 0 and 28 for seronegative animals (Figure 6D). All the dysregulated proteins for this third category are summarized in Table S9.

For CSF analyses, we used a panel consisting of 92 markers with etiology associated with neural injury and neuroinflammation (see www.olink.com). Only three protein markers changed above the 2-fold median change between days 0 and 7 in both groups (Table S10). Meanwhile, between days 0 and 28, a total of 25 markers changed in CSF content level among both groups. The repartition of the dysregulated markers in the CSF is highlighted in Figure 6E. For the seronegative group, 6 proteins met the 2-fold median change cutoff, all were also among the 25 proteins with change in the seropositive group. The markers that show observable increase include interleukin-12 (IL-12), ezrin (EZR), and neuropilin 2 (NRP) (Figure 6F). The increase for IL-12 between the two groups was not statistically significant. All the dysregulated proteins above the 2-fold median change cutoff are summarized in Table S11. Taken together, the protein marker data in both serum and CSF point to differential inflammation, organ damage, and neural injury signatures in NHP based on their anti-AAV9 antibody serology status at the time of AAV9 intra-CSF dosing.

DISCUSSION

AAV-based therapeutics have been transformative for gene therapy, with vectors such as AAV9 currently approved for clinical use in

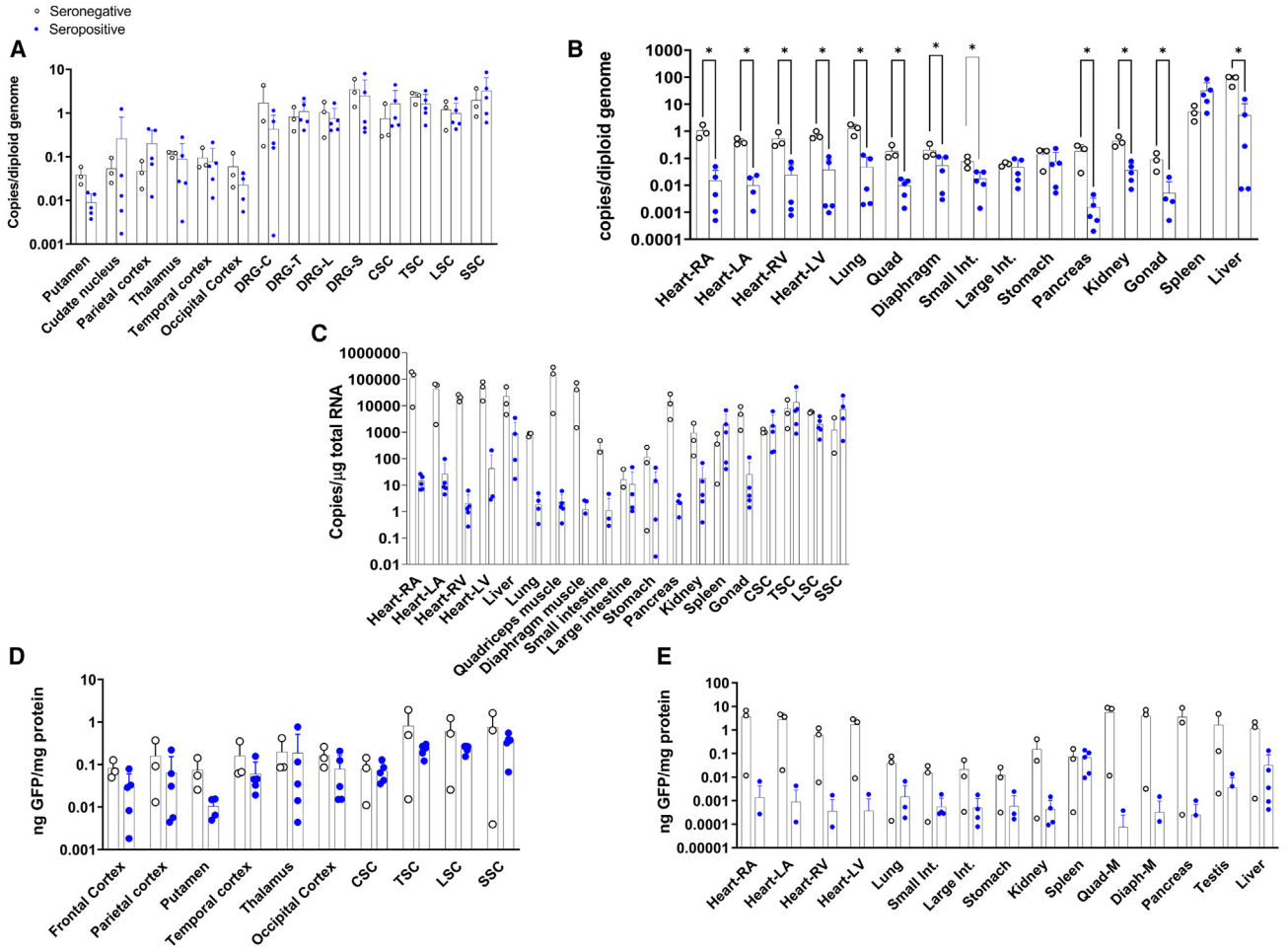

Figure 3. Vector genome biodistribution, GFP mRNA and protein expression in seronegative and seropositive NHPs dosed via lumbar puncture at 5×10^{13} vg with AAV9-GFP vectors and examined for 28 days

Biodistribution of AAV9-GFP vector genomes normalized to reference gene, *CFTR*, in tissues of dosed monkeys at 28 days post-injection. (A) Selected brain regions, spinal cord, and DRG (some brain regions were sampled at multiple locations) and (B) peripheral tissues, for each tissue in each animal, values are averages of three technical replicates and calculated as vg/diploid genome. (C) GFP mRNA level following lumbar puncture dosing of AAV9-GFP. For each tissue in each animal, values are averages of three technical replicates and calculated as copies per μg of total RNA. (D and E) GFP protein quantification as measured by ECLIA. For each tissue in each animal, values are means of two technical replicates and calculated as pg GFP per mg total protein. Animals with protein amount below the level of detection are not represented. All bars represent mean values ± standard deviation (SD). *$p < 0.05$ nonparametric multiple unpaired t tests. Heart-RA, right atrium; Heart-RV, right ventricle; Heart-LA, left atrium; Heart-LV, left ventricle; Int, intestine; DRG, dorsal root ganglion; CSC, cervical spinal cord; TSC, thoracic spinal cord; LSC, lumbar spinal cord; SSC, sacral spinal cord.

spinal muscular atrophy. While some nonclinical data suggest that AAV9 is able to cross the blood-brain barrier after systemic injection,[20,21] delivery to the cerebrospinal fluid vector has been used in several AAV nonclinical and clinical studies[3,9,11,22] since this route provides the option of bypassing the presence of pre-existing anti-AAV9 antibodies and requires lower doses.

Our study seeks to offer a comparative assessment of AAV9 vector transduction efficiency and toxicity markers following intrathecal (LP) delivery of AAV9-GFP in non-human primates with different anti-AAV9 antibody serology status. Binding and neutralizing anti-AAV9 antibodies were not detectable for seronegative monkeys during pre-screening, as observed in Figures 1A and 1B, this underscores high level of concordance between the two assays as reported previously.[18] A previous study had examined the impact of AAV intra-CSF administration in presence of pre-existing antibody in NHP, using doses that was between 2- and 7-fold lower than ours; in addition, two different intra-CSF routes were utilized (cisterna magna or LP) as well as two different AAV serotypes AAV9 and AAV2.5.[4] While our study provides a more complete analyses of potential biomarkers associated with AAV9 intra-CSF dosing, the overall premise of bypassing the presence of pre-existing anti-AAV neutralizing antibodies through AAV intra-CSF dosing for large animals holds true for both studies. Evidence of differences in toxicities associated with

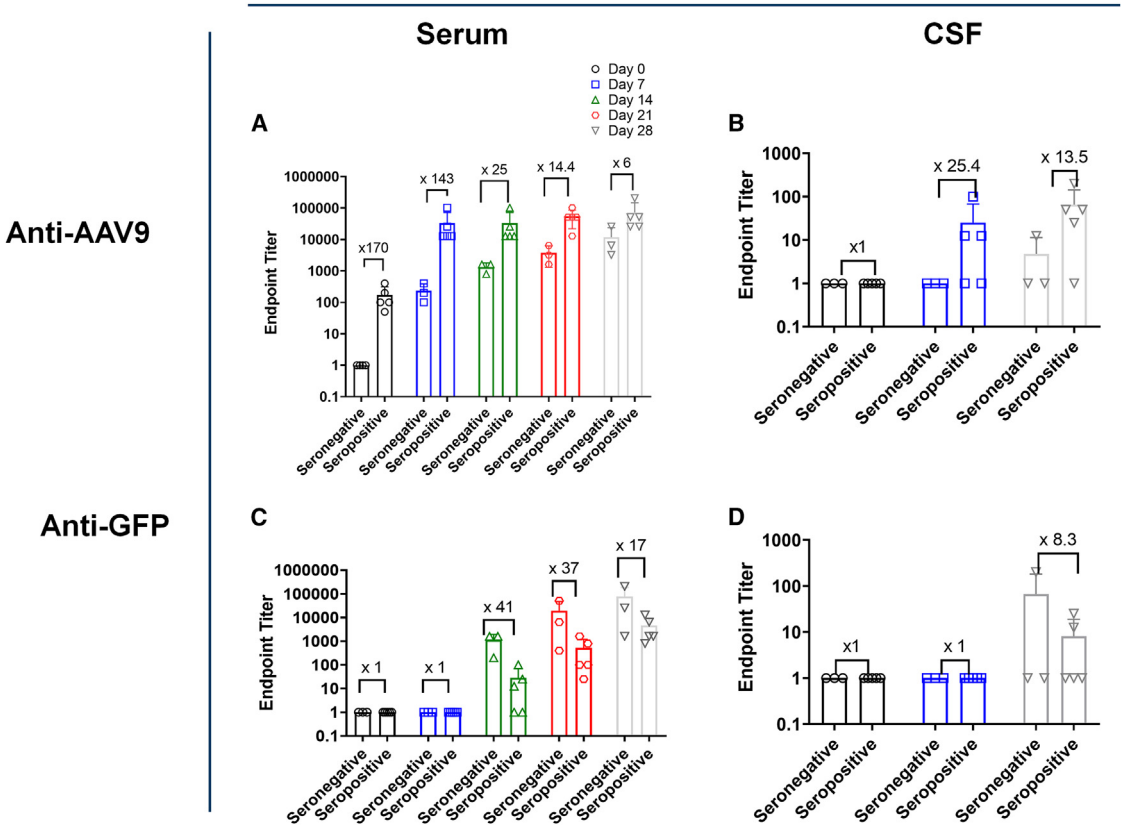

Figure 4. Humoral immune response to the capsid and the GFP transgene in seronegative and seropositive NHPs dosed via lumbar puncture at 5 × 10^{13} vg of AAV9-GFP vectors and examined for 28 days

Endpoint titers of anti-AAV9 (A and B) and anti-GFP (C and D) IgG antibody responses in the serum and CSF samples of seronegative and seropositive NHP. Fold differences in titers between the groups are indicated. All data are presented as mean ± standard deviation (SD). For log graphing purposes, a nominal value of 1 is assigned to all titer endpoints <1:12.5.

the pre-existing AAV9 serology in these monkeys emerged as early as 7 days post-dosing, as indicated by the distinct profile of liver enzymes (Figure 2). We do not clearly know the threshold of vector transduction that triggered elevated liver transaminases; however, these features was also observed in NHP intrathecally treated at doses that were 2- to 4-fold lower but was absent when NHPs received empty AAV9 capsids or promoter-less vectors.[23] Seronegative animals displayed acute elevated transaminases (ALT and AST) activities compared with the seropositive animals. The elevated enzymatic activity of liver transaminases in seronegative animals is consistent with the higher level of the vector transduction (i.e., vector genome, mRNA, and GFP protein) detected in the liver relative to their seropositive counterparts (Figure 3). This difference in the liver, along with the difference in all the other peripheral organs between seronegative and seropositive animals suggest that the presence of neutralizing antibody impacts peripheral organ transduction (Figures 3B, 3C, and 3E). These observations confirm the previous findings that vectors administrated via the intra-CSF route leak into intravascular compartments to disseminate mostly into peripheral organs such as the liver.[15,16] The liver findings in the seropositive group is also in line with the recent publication highlighting that intravenous immunoglobulin (IVIG) administration reduces peripheral liver transduction of intrathecally delivered AAV vector.[24] IVIG pre-treatment and pre-existing AAV antibodies could be considered mitigating strategies for AAV-induced toxicity for intrathecally delivered vectors in clinical settings.

The differential pattern in anti-AAV9 antibody response in the serum for these two groups also reflects their distinct anti-AAV9 antibody serology at the dosing time. Two logs difference in anti-AAV9 IgG antibody titer that favors the seropositive group as early as day 7 post-dosing is reminiscent of a vaccine boost that occurs in pre-immune subjects upon secondary exposure to the same antigen[25,26] (Figure 4A). The contrasting anti-GFP antibody response between the two groups may also reflect the difference in the dissemination of GFP protein in peripheral organs that trended several logs higher for seronegative monkeys. Overall, the amplitude and robustness of the antibody responses to AAV9 and GFP in the serum contrast with the tepid antibody responses detected in the CSF, consistent with previous reports.[12,15]

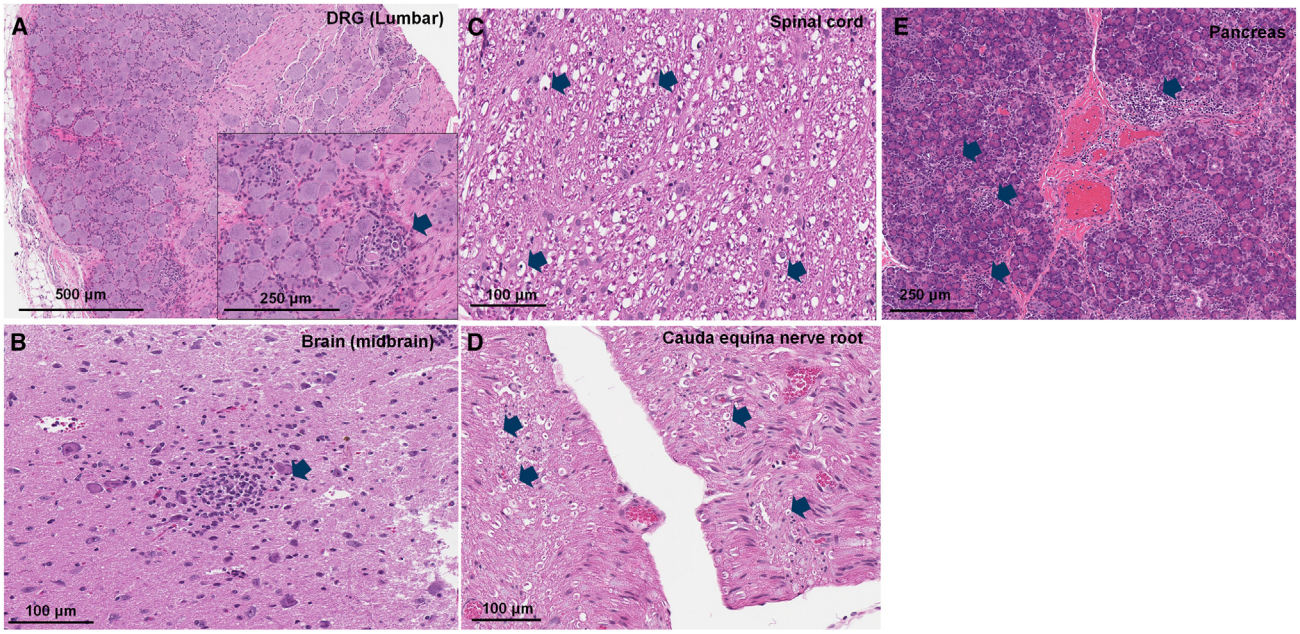

Figure 5. Histopathology analyses, representative images of AAV9-related microscopic findings in the DRG, mid brain, spinal cord, and pancreas in AAV9 seronegative and seropositive NHPs dosed via lumbar puncture at 5 × 10^{13} vg of AAV9-GFP vectors and examined for 28 days

(A) H&E-stained DRG from a AAV9 seronegative NHP displaying neural cell degeneration and mononuclear cell infiltration (see arrow). (B) H&E-stained midbrain region from an AAV9 seronegative NHP displaying evidence of gliosis (see arrow). (C) H&E-stained lumbar spinal cord and (D) sacral spinal cord/nerve root, displaying evidence of axonal degeneration from a AAV9 seropositive NHP (see arrow). (E) H&E-stained pancreas from an AAV9 seronegative NHP with evidence of mononuclear cell infiltration (see arrow).

We used immunoassays and multiplex proteomics to delineate differences in protein levels in the serum and CSF for both groups. Many of the markers that changed noticeably in both groups from day 0 to 28 tended to be chemokines, such as CXCL9, CXCL10, or CXCL11. This observation is in alignment with the previous reports showing that the administration of AAV vectors carrying GFP transgene induces infiltration of neutrophils, CD11+ cells, and other inflammatory cells that secrete chemokines akin to those detected by the OLINK platforms.[27,28] Our data also showed that most of the chemokines detected in the serum tended to be more present in seronegative animals (Figures 6B and 6D); this may be underscored by the fact that more vector and GFP protein dissemination was detected in this group's peripheral organs, leading to more inflammatory events.

Troponin I3, cardiac type (TNNI3), and FK506 binding protein prolyl isomerase 1B (*FKBP1B*) were the most upregulated markers associated with organ damage in seronegative and seropositive animals, respectively (Figures 6B and 6C; Tables S7 and S8). These two markers and others uniquely present in the respective groups may suggest distinct pathways of AAV-induced toxicity based upon the absence or presence of anti-AAV9 pre-existing antibodies. Elevated levels of TNNI3 protein in the serum are often associated with cardiac injuries.[29,30]Alternatively, FKBP1B expression is associated with autophagy.[31] GFP transgene or/and viral capsid-induced inflammation through the stimulation of interferon gene pathways following AAV administration could trigger autophagy pathways as an adaptive response to tissue injury.[32,33] Proteomic analysis of the CSF following intrathecal/LP AAV9 delivery in monkeys also reveals similarities and differences in levels of neuroinflammatory markers between seronegative and seropositive groups. More protein markers were dysregulated above the 2-fold cutoff in seropositive monkey CSF compared with the seronegative ones. The top dysregulated markers that appeared in both groups included IL-12, EZR, and NRP. Activated macrophages (CD68+) and other cell infiltrates known as a primary source of IL-12 have been documented in the CNS and DRG following IT AAV vector delivery in NHP.[34] The elevated presence of IL-12 in the CSF is consistent with the increased incidence of mononuclear inflammatory cells in the DRG and the brain described in the histopathology analyses, likely the result of immune reaction against AAV9 or/and GFP (Figure 5; Tables S2–S4). Evidence of IL-12 production in sensory DRG neurons in mouse has also been reported.[35] Neurodegeneration and axonopathy were noticed for both groups and coincide with elevated NfL chain levels in the CSF (Table S5) along with other structural neural proteins such as ezrin and neuropillin 2 (Table S11). NfL has recently been used to track DRG-related toxicity following AAV9 vector intrathecal delivery in rodents and NHP,[36,37] and is also a biomarker of various neural stressors in human diseases and animal models.[38–40] We do not know yet if these differences suggest more propensity to neural injury for seropositive animals, but they may deserve more investigations in the future. Proteomic analyses in the CSF also revealed noticeable (not statistically significant) elevated levels of NMNAT1 and CD38 in both groups (Figure 6F; Table S11). These two markers are products of the nicotinamide adenine dinucleotide metabolic pathway

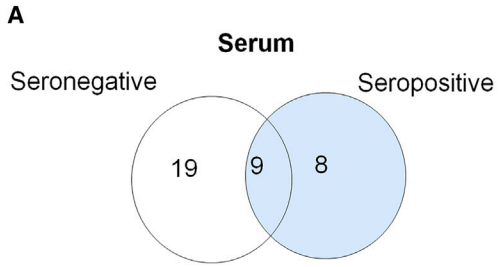

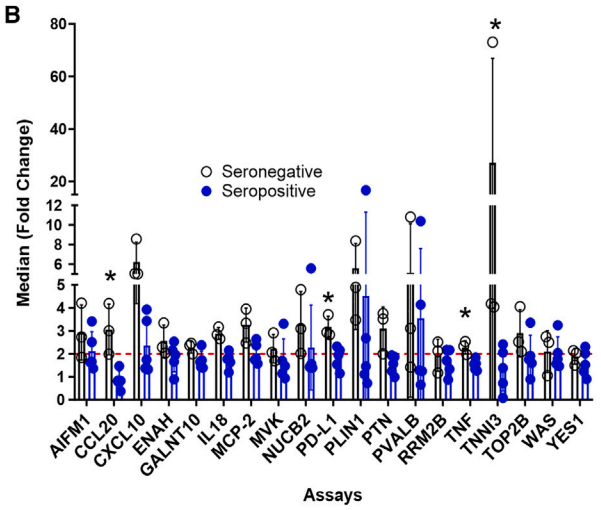

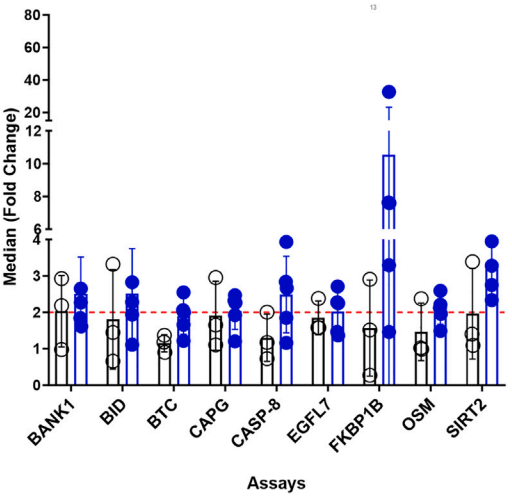

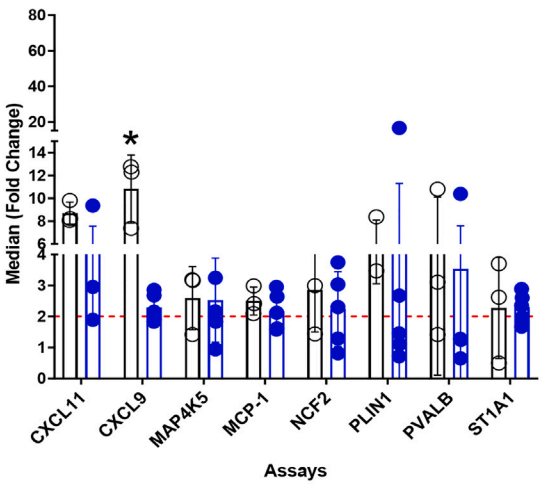

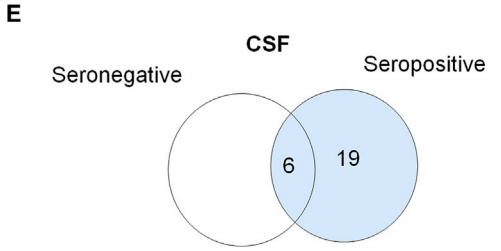

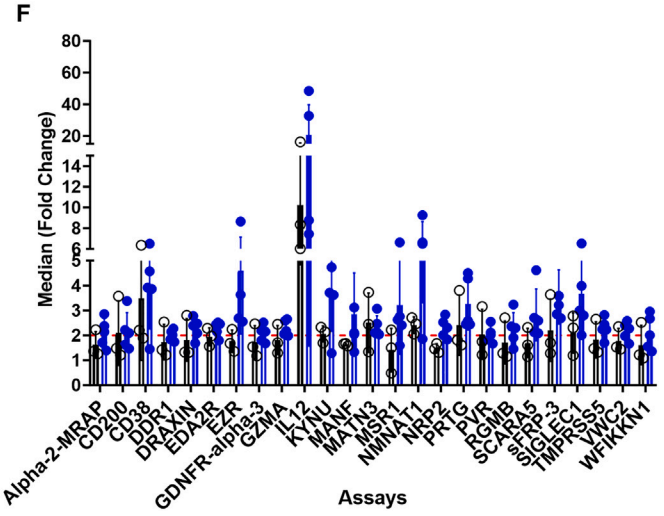

(legend on next page)

implicated in neuroinflammation and neurodegeneration, causative of neural injury.[41–43] Their detection in CSF is consistent with some of the histopathology findings highlighted for CNS and DRG (Tables S2 and S3). Overall, the changes in expression level of these markers beyond the observational time of this study could be investigated in longer studies.

In summary, this study provides a comparative analysis of protein markers, toxicity, and efficacy endpoints in non-human primates with differing pre-existing AAV9 immunity status. This difference in anti-AAV9 pre-existing neutralizing antibodies prior to dosing drive the divergent biodistribution between these two groups, which likely drove the observed toxicity more acutely present in seronegative animals. The relatively small number of animals enrolled in the study, the limited observation time (28 days), and the use of non-self-protein such as GFP could have confounded some of the findings highlighted in this study. In addition, the data presented in this manuscript may be specific to the AAV9 serotype, the relatively high dose applied and the specific range of neutralizing anti-AAV9 antibodies present in these animals. Other serotypes, a different transgene, as well as a different dose in a different anti-AAV serology and/or seroconversion range could have presented a different study outcome. It does not, however, preclude us from concluding that the presence or the absence of pre-existing anti-AAV9 neutralizing antibodies in intrathecally AAV9-GFP-dosed subjects could lead to divergent biodistribution and subsequent AAV-induced toxicity profiles. It is not clear, yet the extent to which these findings will vary based on the level of pre-existing immunity (i.e., higher level of neutralizing anti-AAV9 antibodies). Also of importance in this study is the fact that the presence of anti-AAV9 antibody for intra-CSF dosing appears to be protective to AAV-induced toxicity in the liver, which may be beneficial to dosed subjects in clinical settings. Over the past few years, there have been an increasing number of nonclinical and clinical studies using intra-CSF administration for AAV-based therapeutics. All these studies have varying anti-AAV9 serology eligibility. Our study may be relevant for interpreting toxicity and efficacy analyses that may emerge from these nonclinical and clinical studies.

MATERIALS AND METHODS

NHP studies

The study protocol described in this article and all associated procedures were reviewed and approved by the Mannheimer Foundation Animal Care and Use Committee and were compliant with applicable animal welfare acts, including the Animal Welfare Act, the Guide for the Care and Use of Laboratory Animals, and the Office of Laboratory Animal Welfare. The Mannheimer Foundation is fully accredited by the Animal Association for Accreditation of Laboratory Animal Care. Eight cynomolgus macaques of Mauritian origin (~3 years old, under 6 kg) bred at the Mannheimer Foundation Haman Ranch facility in Florida were used. Animals were screened for anti-AAV9 antibodies using the ELISA-based binding assay adapted from previously published methods.[20] The selected animals were transferred to the Mannheimer Foundation procedural facility in Homestead, Florida.

AAV9-GFP vector

The test article for this study was a self-complementary AAV9-CB-GFP encoding the enhanced GFP gene with the CB promoter (cytomegalovirus [CMV] early enhancer and a hybrid CMV enhancer/chicken β-actin promoter) driving the transcription of vector DNA. Additional elements include a simian virus 40-derived intron and bovine growth hormone polyadenylation signal. The vector was used at concentrations of 5.0×10^{13} vg/mL, diluted in 20 mM Tris buffer with 1 mM $MgCl_2$, 200 mM NaCl, and 0.005% poloxamer 188 (pH 8.1 ± 0.1) at 20°C. The vector used in this study was produced using preclinical research standards that met acceptance and release criteria for *in vivo* research use for the percentage of empty capsid and total purity, number of process-related impurities, plasmid DNA or production cells, endotoxin concentrations, and osmolality.

LP AAV9 vector delivery

On the day of infusion (day 0), animals were given a single intrathecal injection of AAV9-GFP, 5.0×10^{13} vg per animal in a total volume of 1 mL. The dose was intended to mimic high-level IT dosage of AAV9 therapeutics in line with current or past nonclinical program in our organization, but also in the range of several intra-CSF AAV-directed clinical trials.[44] The injection was performed by LP into the subarachnoid space of the lumbar thecal sac. Subjects were placed in the lateral decubitus position and the posterior midline injection site at ~ L4/5 level. Under sterile conditions, a spinal or hypodermic needle with stylet was inserted, and subarachnoid cannulation was confirmed with the backflow of clear CSF from the needle. Approximately 1 mL of CSF was drained, collected, and frozen as baseline samples. This removal of CSF alleviates the pressure increase that the subsequent injection of the AAV vectors would have created. In addition, the animals were tilted in the Trendelenburg position

Figure 6. Protein level analyses in the serum and CSF samples of seronegative and seropositive NHP dosed via lumbar puncture at 5×10^{13} vg with AAV9-GFP vectors and examined for 28 days

(A) Summary of the number of protein markers with differing levels in the serum of seronegative and seropositive animals. Thirty-six out of 184 protein markers in the combined inflammation and organ damage panels changed by at least a median 2-fold between days 0 and 28. Nineteen and eight of these protein markers are uniquely dysregulated in seronegative and seropositive animals, respectively; nine protein markers are dysregulated in both groups. (B) Protein markers with differential level content above the 2-fold threshold in the seronegative and (C) the seropositive animals. (D) Protein markers with differential content level above the 2-fold threshold in both seropositive and seronegative animals. (E) Summary of the number of protein markers with differing content levels in the CSF of the seronegative and seropositive animals. Twenty-five out of 92 protein markers in the neurology panel changed by at least a median 2-fold between days 0 and 28. Six in the seronegative group were also included in the 25 in the seropositive group. (F) Protein markers with differential content level above the 2-fold threshold in seronegative or seropositive animals. All data are expressed as median fold change between days 0 and 28 (± standard deviation) ($n = 3$ for seronegative NHP and $n = 5$ for seropositive NHP). *$p < 0.05$ nonparametric unpaired t test. The red dotted line highlights the 2-fold change threshold, which for a given protein marker conveys the change in relation to their seronegative or seropositive status.

(mild head-down) for 5–10 min to improve the rostral flow distribution of the vector.

Clinical pathology

Clinical pathology that covers hematology, coagulation, and clinical chemistry assessments was performed on the day of dosing (day 0, prior vector administration) and after that weekly (days 7, 14, 21, and 28 post-vector delivery).

Droplet digital PCR

Various tissues were processed for vector genome and mRNA biodistribution. In brief, sample tissues were collected, frozen in liquid nitrogen, and stored at −80°C until analyzed. For vector genome analysis, collected tissues were analyzed using droplet digital PCR (ddPCR) quantitation with a C1000 Thermal Cycler (Bio-Rad). Specific primers and probes used for the ddPCR analysis have been described previously.[16,45] To evaluate the number of AAV9-GFP vector genomes, a two-copy reference gene (*CFTR*) was also quantified for normalization purposes. *CFTR* primers and probe were added to the master mix along with AAV9-GFP primers and probe. AAV9-GFP genomes and *CFTR* genes were quantified in the same reaction using multiplex ddPCR. The resulting values of AAV9-GFP were presented as vg/diploid genome, thus normalizing vector genomes to the *cftr* reference gene. Expression of GFP mRNA transcript was also assessed in the collected tissues using RT-PCR and total RNA was isolated using QIAGEN RNeasy (QIAGEN, Valencia, CA). mRNA was reverse transcribed and quantified during the one-step ddPCR with multiplex primer and probes specific to GFP and GAPDH.

ECL/MSD assay for GFP protein quantification

Green fluorescent protein (GFP) expression was quantified in tissue samples using an ECL assay as described previously.[16] In brief, each collected tissue was immersed in 250 μL of pre-chilled complete protein extraction buffer (pre-chilled T-PER tissue extraction reagent [Thermo Fisher Scientific] with 1× Halt protease inhibitor [Thermo Fisher Scientific]). Tissues were then homogenized using a TissueLyser (QIAGEN) at 30 Hz for 2 min. After centrifugation at 10,000 × *g* and 4°C for 20 min, protein lysates were transferred to a new tube and stored at −20°C until use. According to the manufacturer's protocol, the protein was quantified using the Rapid Gold BCA Protein Assay Kit (Thermo Fisher Scientific). For GFP quantification, 96-well plates were coated by adding 25 μL of mouse anti-GFP monoclonal capture antibody (diluted 10 μg/mL in phosphate-buffered saline [PBS]) overnight at 4°C. After washing three times with 250 μL of PBS-T wash buffer (0.5% Tween 20/PBS), 150 μL of MSD Blocker A was added to each well and incubated on a shaker set to 500 rpm. After shaking at 500 rpm for 1–2 h at room temperature, 25 μL of prepared standards (serial dilutions of GFP recombinant protein) or samples was added to each well. After being shaken for 1–2 h at room temperature, the wells were washed three times with PBS-T, incubated with 25 μL of rabbit anti-GFP polyclonal detection antibody diluted 1:10,000 in the antibody dilution buffer (1.5 mg/mL mouse γ-globulin, 2.5% bovine serum albumin, 0.025% Tween 20/PBS) and incubated while shaking for 1–2 h at room temperature. The wells were washed three times with PBS-T and then incubated in MSD SULFO-TAG anti-rabbit secondary antibody (Meso Scale Discovery) diluted to 0.5 μg/mL in antibody dilution buffer for 1 h while shaking at room temperature. After washing three times with PBS-T, 150 μL of read buffer was added to each well, and the plates were analyzed using a MESO Quick Plex SQ 120 (Meso Scale Discovery). Recombinant GFP was serially diluted before assaying to determine the limit of quantitation and generate a standard curve. The limit of quantification was determined to be 0.024 ng/mL GFP protein in the assay.

Pro-inflammatory cytokines (INF-γ, IL-1β, IL-2, IL-6, IL-8, and IL10), NfL, and neopterin

Serum and CSF samples of treated NHP collected from the femoral vein and from PL, respectively, were analyzed for the presence of inflammatory cytokines using MSD multi-spot assay system pro-inflammatory panel-1 (NHP) and NfL MSD kits following the manufacturer's instructions. Samples were evaluated for neopterin expression using the neopterin ELISA Kit from mybiosource.com, following the manufacturer's instructions.

Anti-AAV9 BAb titers

The IgG antibody response to the AAV9 capsid pre- and post-vector dosing was assessed using binding ELISA as described previously.[20] In brief, 2.0×10^{10} vg/mL solution of AAV9 capsids in 1 mM carbonate buffer was coated into a 96-well titer plate and incubated overnight at 4°C. The next day, the plate was washed and blocked with a 5% nonfat milk solution in PBST. Serum or CSF samples were diluted from 1:12.5 to 1:204,800 and incubated at 37°C for 2 h. Wells were washed with PBST and incubated with a horseradish peroxidase (HRP)-conjugated anti-IgG or anti-IgM monkey secondary antibody (Sigma-Aldrich and Rockland) at room temperature for 1 h. The wells were rewashed in PBST and then developed with 3,3′,5,5′-tetramethylbenzidine (TMB). The reaction was stopped by adding hydrochloric acid, and the absorbance (OD) was read at 450 nm on a plate reader. Binding curves were assessed, and titer was estimated as the last dilution with OD reading between 7- and 8-fold over the background.

NAb assay

HEK293-AAVR cells[46] were seeded in a 96-well tissue culture plate with a density of 40,000 cells per well. After 24 h, the neutralization assay was carried out using a 96-well dilution plate (Greiner 780261 MASTERBLOCK). NHP sera were serially diluted 5-fold starting at 1:5 dilution (1:5, 1:25, 1:125, …) in growth medium containing an AAV9-CBA-NanoLuc (Luciferase) vector at concentration of 4E+10 vg/mL. After 1 h of incubation at 37°C in the dilution plate, 100 μL of the AAV/NHP serum mixtures were transferred to each well of the 96-well plate (AAV9/cell MOI 1E+5 vg/cell). Following a 48-h incubation period at 37°C in 5% CO_2, each well was supplemented with 100 μL of Nano-Glo Luciferase Assay substrate and then subjected to bioluminescence reading using a plate reader (CLARIOstar plus, BMG LABTECH).

Anti-GFP transgene antibody titers

The IgG antibody response to the transgene post-vector dosing was assessed using binding ELISA, as described previously.[12] A recombinant GFP protein (0.5 μg/mL) (recombinant Victoria GFP protein from Abcam, Ab84191) in 1 mM carbonate buffer was coated into a 96-well titer plate and incubated overnight at 4°C. The next day, the plate was washed and blocked with a 5% nonfat milk solution in PBST. Sera or CSF were diluted from 1:12.5 to 1:204,800 and incubated at 37°C for 2 h. Wells were washed with PBST and incubated with a HRP-conjugated anti-monkey secondary antibody (Sigma-Aldrich, St. Louis, MO) at room temperature for 1 h. The wells were rewashed in PBST and then developed with TMB. The reaction was stopped by the addition of hydrochloric acid, and the absorbance (OD) was read at 450 nm on a plate reader. Titer was estimated as the last dilution with OD reading 7- to 8-fold the background OD.

Olink proteomic assays

Serum samples were profiled using multiplex, inflammation, and organ damage immunoassay panels, while CSF samples were profiled using a multiplex neurology immunoassay panel. All were developed by Olink proteomics (Uppsala, Sweden) and were human panels with orthogonality to NHP up to 90%. The proximity extension assay (PEA) technology used by the Olink protocol allows up to 90 analytes per panel to be analyzed simultaneously.[47] PEA consists of pairs of oligonucleotide-labeled antibodies binding to their targeted protein. If the two oligonucleotide strands are brought in proximity, they will hybridize pairwise and be amplified using a microfluidic real-time PCR instrument (Biomark HD, Fluidigm). The data are then quality controlled and normalized using an internal extension control and inter-plate control to adjust for intra- and inter-run variations. The final assay readout is presented in normalized protein expression (NPX) values, an arbitrary unit on a log2-scale in which a high value corresponds to high protein expression. All assay validation data (detection limits, intra- and inter-assay precision data, etc.) are available on the manufacturer's website (www.olink.com). For this study, we analyzed the difference in content level for each protein markers between days 0 and 7 or day 28 as defined by the differential NPX (i.e., dNPX), which represents the NPX at days 7 or 28 minus the NPX of the same analyte at day 0 in the serum or the CSF. A cutoff of ±1 dNPX was set, which corresponds to a 2-fold change in levels of a given protein marker between the two time points. All the data are presented as median fold change.

Histopathology

Tissues collected at necropsy were fixed in 10% neutral buffered formalin and then processed to paraffin block. The tissues were subsequently sectioned at a nominal thickness of approximately 4 μm, stained with hematoxylin and eosin, and evaluated microscopically by an American College of Veterinary Pathologists (ACVP) board-certified anatomic veterinary pathologist experienced in toxicologic pathology and neuropathology.

Data analysis and statistics

All data are expressed as median or mean ± standard deviation (SD) and analyzed using prism 9.0 (GraphPad software). The low number of animals used for this study does not lend itself to high-power statistical interpretation; nonetheless, statistical analyses were run to examine differences between the seronegative and seropositive groups using either two-way ANOVA Sidak's multiple comparison test or nonparametric unpaired t test (both using GraphPad, Prism 9). Statistical significance was set as $*p < 0.05$. If not specified, this denotes that no statistical significance was found.

DATA AND CODE AVAILABILITY

All data generated in this study are included in this published article, and in the supplemental section of the manuscript. All these data will be made available upon request.

ACKNOWLEDGMENTS

The authors acknowledge Kevin Foust, Terrence Oday, Mark Milton, Wenbin Qi, Pablo Morales, and the Mannheimer Foundation staff for their support in the execution of this study.

AUTHOR CONTRIBUTIONS

G.H.G. wrote the manuscript and contributed to the study design, the execution of experiments, and did the data collection and analysis. J.D., B.C., R.K., Y.G., and X.L. contributed to the execution of the experiments, the collection, the analysis, and the interpretation of the data. F.O. edited the manuscript and contributed to data interpretation. T.M. contributed to the data interpretation and to the editing and review of the manuscript.

DECLARATION OF INTERESTS

All the authors are current and past employees of Novartis Gene Therapies (G.H.G., J.D., Y.G., B.C., and F.O.) and Novartis Biomedical Research (G.H.G., F.O., R.K., and T.M.). All authors disclose salaries and compensations received for the execution of this study funded by Novartis Gene Therapies and Novartis Biomedical Research.

SUPPLEMENTAL INFORMATION

Supplemental information can be found online at https://doi.org/10.1016/j.omtm.2024.101371.

REFERENCES

1. Nidetz, N.F., McGee, M.C., Tse, L.V., Li, C., Cong, L., Li, Y., and Huang, W. (2020). Adeno-associated viral vector-mediated immune responses: Understanding barriers to gene delivery. Pharmacol. Ther. *207*, 107453. https://doi.org/10.1016/j.pharmthera.2019.107453.

2. Costa Verdera, H., Kuranda, K., and Mingozzi, F. (2020). AAV Vector Immunogenicity in Humans: A Long Journey to Successful Gene Transfer. Mol. Ther. *28*, 723–746. https://doi.org/10.1016/j.ymthe.2019.12.010.

3. Federici, T., Taub, J.S., Baum, G.R., Gray, S.J., Grieger, J.C., Matthews, K.A., Handy, C.R., Passini, M.A., Samulski, R.J., and Boulis, N.M. (2012). Robust spinal motor neuron transduction following intrathecal delivery of AAV9 in pigs. Gene Ther. *19*, 852–859. https://doi.org/10.1038/gt.2011.130.

4. Gray, S.J., Nagabhushan Kalburgi, S., McCown, T.J., and Jude Samulski, R. (2013). Global CNS gene delivery and evasion of anti-AAV-neutralizing antibodies by intrathecal AAV administration in non-human primates. Gene Ther. *20*, 450–459. https://doi.org/10.1038/gt.2012.101.

5. Hinderer, C., Bell, P., Vite, C.H., Louboutin, J.P., Grant, R., Bote, E., Yu, H., Pukenas, B., Hurst, R., and Wilson, J.M. (2014). Widespread gene transfer in the central nervous system of cynomolgus macaques following delivery of AAV9 into the cisterna magna. Mol. Ther. Methods Clin. Dev. *1*, 14051. https://doi.org/10.1038/mtm.2014.51.

6. Hinderer, C., Bell, P., Katz, N., Vite, C.H., Louboutin, J.P., Bote, E., Yu, H., Zhu, Y., Casal, M.L., Bagel, J., et al. (2018). Evaluation of Intrathecal Routes of Administration

for Adeno-Associated Viral Vectors in Large Animals. Hum. Gene Ther. *29*, 15–24. https://doi.org/10.1089/hum.2017.026.

7. Hordeaux, J., Hinderer, C., Goode, T., Katz, N., Buza, E.L., Bell, P., Calcedo, R., Richman, L.K., and Wilson, J.M. (2018). Toxicology Study of Intra-Cisterna Magna Adeno-Associated Virus 9 Expressing Human Alpha-L-Iduronidase in Rhesus Macaques. Mol. Ther. Methods Clin. Dev. *10*, 79–88. https://doi.org/10.1016/j.omtm.2018.06.003.
8. Hinderer, C., Bell, P., Gurda, B.L., Wang, Q., Louboutin, J.P., Zhu, Y., Bagel, J., O'Donnell, P., Sikora, T., Ruane, T., et al. (2014). Intrathecal gene therapy corrects cns pathology in a feline model of mucopolysaccharidosis. Mol. Ther. *22*, 2018–2027. https://doi.org/10.1038/mt.2014.135.
9. Marcó, S., Haurigot, V., Jaén, M.L., Ribera, A., Sánchez, V., Molas, M., Garcia, M., León, X., Roca, C., Sánchez, X., et al. (2021). Seven-year follow-up of durability and safety of AAV CNS gene therapy for a lysosomal storage disorder in a large animal. Mol. Ther. Methods Clin. Dev. *23*, 370–389. https://doi.org/10.1016/J.OMTM.2021.09.017.
10. Beharry, A., Gong, Y., Kim, J.C., Hanlon, K.S., Nammour, J., Hieber, K., Eichler, F., Cheng, M., Stemmer-Rachamimov, A., Stankovic, K.M., et al. (2022). The AAV9 Variant Capsid AAV-F Mediates Widespread Transgene Expression in Nonhuman Primate Spinal Cord after Intrathecal Administration. Hum. Gene Ther. *33*, 61–75. https://doi.org/10.1089/hum.2021.069.
11. Samaranch, L., Sebastian, W.S., Kells, A.P., Salegio, E.A., Heller, G., Bringas, J.R., Pivirotto, P., Dearmond, S., Forsayeth, J., and Bankiewicz, K.S. (2014). AAV9-mediated expression of a non-self-protein in nonhuman primate central nervous system triggers widespread neuroinflammation driven by antigen-presenting cell transduction. Mol. Ther. *22*, 329–337. https://doi.org/10.1038/mt.2013.266.
12. Ramsingh, A.I., Gray, S.J., Reilly, A., Koday, M., Bratt, D., Koday, M.T., Munson, P., Murnane, R., Smedley, J., Hu, Y., et al. (2018). Sustained AAV9-mediated expression of a non-self-protein in the CNS of non-human primates after immunomodulation. PLoS One *13*, e0198154. https://doi.org/10.1371/journal.pone.0198154.
13. Meadows, A.S., Pineda, R.J., Goodchild, L., Bobo, T.A., and Fu, H. (2019). Threshold for Pre-existing Antibody Levels Limiting Transduction Efficiency of Systemic rAAV9 Gene Delivery: Relevance for Translation. Mol. Ther. Methods Clin. Dev. *13*, 453–462. https://doi.org/10.1016/j.omtm.2019.04.004.
14. Fu, H., Meadows, A.S., Pineda, R.J., Kunkler, K.L., Truxal, K.V., McBride, K.L., Flanigan, K.M., and McCarty, D.M. (2017). Differential prevalence of antibodies against adeno-associated virus in healthy children and patients with mucopolysaccharidosis III: perspective for AAV-mediated gene therapy. Hum. Gene Ther. Clin. Dev. *28*, 187–196. https://doi.org/10.1089/hum.2017.109.
15. Bey, K., Deniaud, J., Dubreil, L., Joussemet, B., Cristini, J., Ciron, C., Hordeaux, J., Le Boulc'h, M., Marche, K., Maquigneau, M., et al. (2020). Intra-CSF AAV9 and AAVrh10 Administration in Nonhuman Primates: Promising Routes and Vectors for Which Neurological Diseases? Mol. Ther. Methods Clin. Dev. *17*, 771–784. https://doi.org/10.1016/j.omtm.2020.04.001.
16. Meseck, E.K., Guibinga, G., Wang, S., McElroy, C., Hudry, E., and Mansfield, K. (2022). Intrathecal sc-AAV9-CB-GFP: Systemic Distribution Predominates Following Single-Dose Administration in Cynomolgus Macaques. Toxicol. Pathol. *50*, 415–431. https://doi.org/10.1177/01926233221101309.
17. Schulz, M., Levy, D.I., Petropoulos, C.J., Bashirians, G., Winburn, I., Mahn, M., Somanathan, S., Cheng, S.H., and Byrne, B.J. (2023). Binding and neutralizing anti-AAV antibodies: Detection and implications for rAAV-mediated gene therapy. Mol. Ther. *31*, 616–630. https://doi.org/10.1016/j.ymthe.2023.01.010.
18. Gardner, M.R., Mendes, D.E., Muniz, C.P., Martinez-Navio, J.M., Fuchs, S.P., Gao, G., and Desrosiers, R.C. (2022). High concordance of ELISA and neutralization assays allows for the detection of antibodies to individual AAV serotypes. Mol. Ther. Methods Clin. Dev. *24*, 199–206. https://doi.org/10.1016/j.omtm.2022.01.003.
19. Meliani, A., Leborgne, C., Triffault, S., Jeanson-Leh, L., Veron, P., and Mingozzi, F. (2015). Determination of anti-adeno-associated virus vector neutralizing antibody titer with an in vitro reporter system. Hum. Gene Ther. Methods *26*, 45–53. https://doi.org/10.1089/hgtb.2015.037.
20. Bevan, A.K., Duque, S., Foust, K.D., Morales, P.R., Braun, L., Schmelzer, L., Chan, C.M., McCrate, M., Chicoine, L.G., Coley, B.D., et al. (2011). Systemic gene delivery in large species for targeting spinal cord, brain, and peripheral tissues for pediatric disorders. Mol. Ther. *19*, 1971–1980. https://doi.org/10.1038/mt.2011.157.
21. Foust, K.D., Nurre, E., Montgomery, C.L., Hernandez, A., Chan, C.M., and Kaspar, B.K. (2009). Intravascular AAV9 preferentially targets neonatal neurons and adult astrocytes. Nat. Biotechnol. *27*, 59–65. https://doi.org/10.1038/nbt.1515.
22. Duque, S., Porensky, P., William, D.A., Odermatt, P., Nlend, R.N., Bevan, A.K., Foust, K., Braun, L., Schmelzer, L., Schumperli, D., et al. (2013). O.8 Intrathecal delivery of AAV9 vectors to model and rescue a large animal model of SMA. Neuromuscul. Disord. *23*, 797. https://doi.org/10.1016/j.nmd.2013.06.558.
23. Hudry, E., Aihara, F., Meseck, E., Mansfield, K., McElroy, C., Chand, D., Tukov, F.F., and Penraat, K. (2023). Liver injury in cynomolgus monkeys following intravenous and intrathecal scAAV9 gene therapy delivery. Mol. Ther. *31*, 2999–3014. https://doi.org/10.1016/J.YMTHE.2023.07.020.
24. Horiuchi, M., Hinderer, C.J., Greig, J.A., Dyer, C., Buza, E.L., Bell, P., Chichester, J.A., Hayashi, P.M., Yan, H., Goode, T., and Wilson, J.M. (2022). Intravenous immunoglobulin prevents peripheral liver transduction of intrathecally delivered AAV vectors. Mol. Ther. Methods Clin. Dev. *27*, 272–280. https://doi.org/10.1016/J.OMTM.2022.09.017.
25. Palgen, J.L., Feraoun, Y., Dzangué-Tchoupou, G., Joly, C., Martinon, F., Le Grand, R., and Beignon, A.S. (2021). Optimize Prime/Boost Vaccine Strategies: Trained Immunity as a New Player in the Game. Front. Immunol. *12*, 612747. https://doi.org/10.3389/fimmu.2021.612747.
26. Pollard, A.J., and Bijker, E.M. (2021). A guide to vaccinology: from basic principles to new developments. Nat. Rev. Immunol. *21*, 83–100. https://doi.org/10.1038/s41577-020-00479-7.
27. Zaiss, A.-K., Liu, Q., Bowen, G.P., Wong, N.C.W., Bartlett, J.S., and Muruve, D.A. (2002). Differential Activation of Innate Immune Responses by Adenovirus and Adeno-Associated Virus Vectors. J. Virol. *76*, 4580–4590. https://doi.org/10.1128/jvi.76.9.4580-4590.2002.
28. Zaiss, A.K., and Muruve, D.A. (2008). Immunity to adeno-associated virus vectors in animals and humans: A continued challenge. Gene Ther. *15*, 808–816. https://doi.org/10.1038/gt.2008.54.
29. Fathil, M.F.M., Md Arshad, M.K., Gopinath, S.C.B., Hashim, U., Adzhri, R., Ayub, R.M., Ruslinda, A.R., Nuzaihan M N, M., Azman, A.H., Zaki, M., and Tang, T.H. (2015). Diagnostics on acute myocardial infarction: Cardiac troponin biomarkers. Biosens. Bioelectron. *70*, 209–220. https://doi.org/10.1016/j.bios.2015.03.037.
30. Missov, E., Calzolari, C., and Pau, B. (1997). Circulating cardiac troponin I in severe congestive heart failure. Circulation *96*, 2953–2958. https://doi.org/10.1161/01.CIR.96.9.2953.
31. Xu, Y., Li, R., Li, X., Dong, N., Wu, D., Hou, L., Yin, K., and Zhao, C. (2020). An Autophagy-Related Gene Signature Associated with Clinical Prognosis and Immune Microenvironment in Gliomas. Front. Oncol. *10*, 571189. https://doi.org/10.3389/fonc.2020.571189.
32. Hu, Q., Knight, P.H., Ren, Y., Ren, H., Zheng, J., Wu, X., Ren, J., and Sawyer, R.G. (2019). The emerging role of stimulator of interferons genes signaling in sepsis: Inflammation, autophagy, and cell death. Acta Physio *225*, e13194. https://doi.org/10.1111/apha.13194.
33. Sun, F., Liu, Z., Yang, Z., Liu, S., and Guan, W. (2019). The emerging role of STING-dependent signaling on cell death. Immunol. Res. *67*, 290–296. https://doi.org/10.1007/s12026-019-09073-z.
34. Guibinga, G.H., Johnson, E., Le, J., Penraat, K., Hudry, E., Meseck, E., McElroy, C., Ozsolak, F., and Mansfield, K. (2022). Differential Histopathological and Proteomics Changes in Doral Root Ganglia (DRG) of Cynomolgus Macaques Following Intrathecal (IT) Delivery of Empty AAV9 Capsids, and AAV9 Carrying Transcriptionally Active or Inert Cargo. ASGCT-2022, Abstracts (# 1208). Mol. Ther. *30*, 562. https://doi.org/10.1016/J.YMTHE.2022.04.017.
35. Hikawa, N., Ishikawa, Y., and Takenaka, T. (2004). Interleukin-12 p40-homodimer production in sensory dorsal root ganglion neurons. Neuroscience *129*, 75–83. https://doi.org/10.1016/j.neuroscience.2004.07.035.
36. Johnson, E.W., Sutherland, J.J., Meseck, E., McElroy, C., Chand, D.H., Tukov, F.F., Hudry, E., and Penraat, K. (2023). Neurofilament light chain and dorsal root ganglia injury after adeno-associated virus 9 gene therapy in nonhuman primates. Mol. Ther. Methods Clin. Dev. *28*, 208–219. https://doi.org/10.1016/J.OMTM.2022.12.012.

37. Fader, K.A., Pardo, I.D., Kovi, R.C., Somps, C.J., Wang, H.H., Vaidya, V.S., Ramaiah, S.K., and Sirivelu, M.P. (2022). Circulating neurofilament light chain as a promising biomarker of AAV-induced dorsal root ganglia toxicity in nonclinical toxicology species. Mol. Ther. Methods Clin. Dev. *25*, 264–277. https://doi.org/10.1016/j.omtm.2022.03.017.

38. Verde, F., Otto, M., and Silani, V. (2021). Neurofilament Light Chain as Biomarker for Amyotrophic Lateral Sclerosis and Frontotemporal Dementia. Front. Neurosci. *15*, 679199. https://doi.org/10.3389/fnins.2021.679199.

39. Gaetani, L., Blennow, K., Calabresi, P., Di Filippo, M., Parnetti, L., and Zetterberg, H. (2019). Neurofilament light chain as a biomarker in neurological disorders. J. Neurol. Neurosurg. Psychiatry *90*, 870–881. https://doi.org/10.1136/jnnp-2018-320106.

40. Bacioglu, M., Maia, L.F., Preische, O., Schelle, J., Apel, A., Kaeser, S.A., Schweighauser, M., Eninger, T., Lambert, M., Pilotto, A., et al. (2016). Neurofilament Light Chain in Blood and CSF as Marker of Disease Progression in Mouse Models and in neurodegenerative diseases. Neuron *91*, 56–66. https://doi.org/10.1016/j.neuron.2016.05.018.

41. Sasaki, Y., Araki, T., and Milbrandt, J. (2006). Stimulation of nicotinamide adenine dinucleotide biosynthetic pathways delays axonal degeneration after axotomy. J. Neurosci. *26*, 8484–8491. https://doi.org/10.1523/JNEUROSCI.2320-06.2006.

42. Verghese, P.B., Sasaki, Y., Yang, D., Stewart, F., Sabar, F., Finn, M.B., Wroge, C.M., Mennerick, S., Neil, J.J., Milbrandt, J., and Holtzman, D.M. (2011). Nicotinamide mononucleotide adenylyl transferase 1 protects against acute neurodegeneration in developing CNS by inhibiting excitotoxic-necrotic cell death. Proc. Natl. Acad. Sci. USA *108*, 19054–19059. https://doi.org/10.1073/pnas.1107325108.

43. Guerreiro, S., Privat, A.L., Bressac, L., and Toulorge, D. (2020). CD38 in Neurodegeneration and Neuroinflammation. Cells *9*, 471. https://doi.org/10.3390/cells9020471.

44. Chen, X., Lim, D.A., Lawlor, M.W., Dimmock, D., Vite, C.H., Lester, T., Tavakkoli, F., Sadhu, C., Prasad, S., and Gray, S.J. (2023). Biodistribution of Adeno-Associated Virus Gene Therapy Following Cerebrospinal Fluid-Directed Administration. Hum. Gene Ther. *34*, 94–111. https://doi.org/10.1089/hum.2022.163.

45. Meyer, K., Ferraiuolo, L., Schmelzer, L., Braun, L., McGovern, V., Likhite, S., Michels, O., Govoni, A., Fitzgerald, J., Morales, P., et al. (2015). Improving single injection CSF delivery of AAV9-mediated gene therapy for SMA: A dose-response study in mice and nonhuman primates. Mol. Ther. *23*, 477–487. https://doi.org/10.1038/mt.2014.210.

46. Baatartsogt, N., Kashiwakura, Y., Hayakawa, M., Kamoshita, N., Hiramoto, T., Mizukami, H., and Ohmori, T. (2021). A sensitive and reproducible cell-based assay via secNanoLuc to detect neutralizing antibody against adeno-associated virus vector capsid. Mol. Ther. Methods Clin. Dev. *22*, 162–171. https://doi.org/10.1016/J.OMTM.2021.06.004.

47. Sudhakar, P., Salomon, B., Verstockt, B., Ungaro, R., Aden, K., D'Haens, G., Komori, K., Guay, H., Silverberg, M., Vermeire, S., and Halfvarson, J. (2022). DOP79 Biomarkers for IBD using OLINK Proteomics inflammation panel: Preliminary results from the COLLIBRI consortium. J Crohns Colitis *16*, i123–i124. https://doi.org/10.1093/ecco-jcc/jjab232.118.